SAND2015-9330J

Incorporating physically-based microstructures in materials modeling: Bridging phase field and crystal plasticity frameworks

Hojun Lim[a,*], Fadi Abdeljawad[a], Steven Owen[b], Byron Hanks[b], Corbett C. Battaile[a]

[a] *Computational Materials and Data Science Department, Sandia National Laboratories, Albuquerque NM, 87185, USA*

[b] *Simulation Modeling Sciences Department, Sandia National Laboratories, Albuquerque NM, 87185, USA*

Abstract

The mechanical properties of materials systems are highly influenced by various features at the microstructural level. The ability to capture these heterogeneities and incorporate them into continuum-scale frameworks of the deformation behavior is considered a key step in the development of complex non-local models of failure. In this study, we present a modeling framework that incorporates physically-based realizations of polycrystalline aggregates from a phase field (PF) model into a crystal plasticity finite element (CP-FE) framework. Simulated annealing via the PF model yields ensembles of materials microstructures with various grain sizes and shapes. With the aid of a novel FE meshing technique, FE discretizations of these microstructures are generated, where several key features, such as conformity to interfaces, and triple junction angles, are preserved. The discretizations are then used in the CP-FE framework to simulate the mechanical response of polycrystalline α-iron. It is shown that the conformal discretization across interfaces reduces artificial stress localization commonly observed in voxelated FE discretizations. The work presented herein is a first step towards incorporating physically-based microstructures in lieu of the overly simplified heretofore ones commonly used. In broader terms, the proposed framework provides future avenues to explore bridging models of materials processes, e.g., additive manufacturing and microstructure evolution of multi-phase multi-component systems, into continuum-scale frameworks of the mechanical properties.

Keywords: Phase field, crystal plasticity, finite element method, hex meshing

*Corresponding author
Email address: hnlim@sandia.gov (Hojun Lim)

1. Introduction

It is universally accepted that the physical properties of conventional metallic systems and alloys are attributed to several features, inhomogeneities, at the microstructural level, such as grains with distinct crystallographic orientations, phases of varying compositions, precipitates and their respective topological features (spatial distribution and sizes), internal interfaces and structural defects (Phillips, 2001; Holm and Battaile, 2001; Arzt, 1998); all of which are not generally in global thermodynamic equilibrium. For instance, several metallurgical routes can be followed to strengthen a metallic system, such as alloying (solid solution strengthening), incorporation of second phase particles (hard obstacles or penetrable coherent precipitates), or grain size refinement via the classic Hall-Petch effect (Arzt, 1998; Dieter, 1986; Hirth and Lothe, 1982). In ferromagnetic materials, magnetic microstructures with uniform magnetization form which are separated by domain walls, whose thickness depends on the crystal anisotropy and quantum-mechanical exchange interaction. The interaction of domain walls with non-magnetic particles affects the net coercive force and therefore the magnetic pressure that moves domain walls (Arzt, 1998; Haasen, 1972).

The role of microstructural features, which span many length scales, on the properties at the macroscopic scale falls naturally within the structure-process-property paradigm and has triggered many research efforts across various disciplines to develop microstructure-informed modeling frameworks (Steinhauser and Hiermaier, 2009; Steinhauser, 2008). With regard to the mechanical properties of polycrystalline metals, traditional continuum models do not explicitly account for heterogeneities and effective materials properties are used instead (Nemat-Nasser and Hori, 1993). On the other hand, crystal plasticity (CP) frameworks use constitutive descriptions applied to individual grains in a polycrystalline system and thus microstructural effects, such as grain morphology (grain size and shape) and texture (grain orientation), are directly considered. CP models are widely implemented numerically in finite element frameworks (CP-FE) and are used to predict the mechanical response and texture evolution of polycrystalline aggregates (Peirce et al., 1982; Kalidindi et al., 1992; Anand and Kalidindi, 1994; Delaire et al., 2000; Raabe et al., 2001; Dawson et al., 2003; Zhao et al., 2008). In these models, synthetic microstructures are typically generated, where grain shapes are the output of a tiling (partitioning) protocol such as Voronoi tessellation (VT) (Barbe et al., 2001; Aoyagi and Shizawa, 2007; Zhang et al., 2007; Meier et al., 2014) or other variants

based on it, e.g., multiplicatively weighted VT and k-order VT (Okabe et al., 2000; Boissonnat and Yvinec, 1998). In these algorithms, the simulation domain is initially seeded with spatially uncorrelated points (i.e., centers of fully penetrable disks, Poisson distributed points) (Torquato, 2002) or a spatial correlation is introduced, where seed points represent centers of randomly packed hard spheres (mono-disperse or poly-disperse) (Bishop et al., 2015). Others use tessellation growth models to generate realizations of microstructures, where the cells are allowed to grow/shrink with prescribed velocities (Teferra and Graham-Brady, 2015).

Finite element realizations based on the aforementioned tessellation protocols typically suffer from two shortcomings, which may prove important especially when local effects are used in models of failure/damage, i.e., nucleation of cracks or voids. First, these realizations, albeit easy to generate, are based on tiling algorithms that are not informed by the energetics and thermodynamics of materials processes. With respect to grains in polycrystalline systems, such processes are driven by internal interfaces, i.e., grain boundaries (GBs), whose evolution leads to the reduction of the total free energy, ΔG, via $\Delta G = \Delta(\gamma A)$, where γ and A are the interface energy and area, respectively. Various details emerge from this GB-driven process, such as the Young-Herring condition (Herring, 1951) that sets the angles at triple junctions, where three grains meet, the von Neumann-Mullins kinetic law in two-dimensional isotropic systems (Mullins, 1956; von Neumann, 1952), and its extension to three and higher dimensions by MacPherson and Srolovitz (MacPherson and Srolovitz, 2007). The lack of these thermodynamic considerations in such tiling algorithms results in realizations of microstructures with distributions for the grain volumes and various topological features that do not agree with either experimental observations or meso-scale models of grain microstructures (Lazar et al., 2011, 2010). The second is related to the numerical discretization, within the FE framework, of these microstructures, which yields non-smooth voxelated interfaces between adjoining grains (Barbe et al., 2001). These so-called wedding-cake irregularities in the interface profiles can lead to artificial stress localization, i.e., act as stress concentration sites. Attempts have been focused on the first aspect but not the second (Fromm et al., 2012).

Several models have been developed to investigate interface-driven processes in polycrystalline metallic systems and alloys. These include Potts (Anderson et al., 1984; Srolovitz et al., 1984b,a), level set (Osher and Sethian, 1988), vertex (Kawasaki et al., 1989), phase field (Krill and Chen, 2002; Chen and Yang, 1994; Chen, 2002), Cellular Automata (Liu et al., 1996; Wolfram, 1984),

and front-tracking (Glimm et al., 1998; Hyman, 1984; Lazar et al., 2011, 2010) models. A typical output of these frameworks is realizations of grain microstructures subject to the boundary conditions and interface properties (energy and mobility) used as inputs. In this work, we utilize a recently developed phase field framework for the microstructural evolution of polycrystalline metals to generate ensembles of grain microstructures at several simulated annealing times, and thus various average grain sizes. In contrast to the tetrahedral FE discretization used by Pyle et al. (Pyle et al., 2012), a novel meshing technique is utilized to generate FE discretizations of these microstructures with eight-noded hexahedral elements that conform to the inherent grain topology and ensure smoothness across GBs. The FE-discretized microstructures are then used to simulate the mechanical properties of polycrystalline α-iron via the CP-FE framework. Simulation results of two- (2D) and three-dimensional (3D) systems highlight the effects of the conformal mesh across interfaces on the local mechanical response. In broader terms, our modeling approach provides a first step towards bridging models of materials processes to ones of properties.

The rest of the manuscript is organized as follows: In Sec. 2, an outline is presented of the phase field model for the generation of grain microstructures, conformal meshing technique, and crystal plasticity framework for the mechanical response of polycrystalline materials. Simulations results of various 2D and 3D systems are presented and discussed in Sec. 3. Finally, concluding remarks are presented in Sec. 4

2. Modeling Approach

The theoretical and numerical frameworks used in this work are presented. Our modeling approach is comrpised of three steps. First, the phase field framework is used for simulated annealing, where realizations of grain microstructures are obtained at various simulation times, thus allowing for ensembles with various grain sizes. Next, the novel conformal meshing technique is used to generate FE numerical discretizations, from the phase field results, that preserve grain topologies and ensure smoothness across interfaces between adjoining grains, thus avoiding wedding-cake interfaces. Finally, with the aid of the CP-FE framework, FE discretizations of materials microstructures are used to simulate the mechanical response of polycrystalline α-iron.

2.1. Phase field model for grain microstructures

We employ a recently developed phase field (PF) model of grain microstructures to generate polycrystalline systems with various distributions of grain shapes and sizes. The model is briefly outlined here and the reader is referred to (Abdeljawad and Foiles, 2015; Abdeljawad et al., 2014) for more details on the model. The starting point of the phase field model for grain microstructures is the introduction of structural order parameters (OPs) $\{\phi_i(\mathbf{r},t), i = 1,\cdots,n_\phi\}$ that describe grains with various crystallographic orientations. Here, $\mathbf{r}, t, n_\phi$ denote the position vector, time and number of OPs needed to resolve the microstructure, respectively. Next, a coarse-grained free energy functional of a polycrystalline system, $\mathcal{F}_{tot}$, is given by

$$\mathcal{F}_{tot} = \int d\mathbf{r}\left[W_\phi f_{grain}(\phi_i) + \sum_i^{n_\phi} \frac{\epsilon_i^2}{2}|\nabla\phi_i|^2\right], \tag{1}$$

where $f_{grain}(\phi_i) = f_{grain}(\{\phi_i(\mathbf{r},t), i = 1,\cdots,n_\phi\})$ is the homogeneous free energy density and W_ϕ is a parameter that sets the energy scale. The second term on the right hand side of Eq. (1) describes grain boundary (GB) energy, where under the isotropy assumption $\epsilon_i = \epsilon$. The OPs are conveniently chosen such that the equilibrium values within a grain $\{\phi_i(\mathbf{r},t) = 1, \phi_{j\neq i}(\mathbf{r},t) = 0, i,j = 1,\cdots,n_\phi\}$. Herein, we adopt the following form for the free energy density of a grain microstructure

$$f_{grain} = \frac{4}{3}\left[1 - 4\sum_{i=1}^{n_\phi}\phi_i^3 + 3\left(\sum_{i=1}^{n_\phi}\phi_i^2\right)^2\right], \tag{2}$$

where again the minima of f_{grain} are located at $\{\phi_i\} = \{1,0,\cdots,0\} = \cdots = \{0,0,\cdots,1\}$.

Within the Ginzburg-Landau formalism and with the aid of variational principles, the spatio-temporal evolution of the OPs $\{\phi_i(\mathbf{r},t), i = 1,\cdots,n_\phi\}$ follows from the Allen-Cahn equation (Allen and Cahn, 1979):

$$\frac{\partial\phi_i}{\partial t} = -L_i\left(\frac{\delta\mathcal{F}_{tot}}{\delta\phi_i}\right),\ i = 1,\cdots,n_\phi, \tag{3}$$

where the model parameters L_i, one for each ϕ_i, control GB mobility. Here, the isotropy assumption of GB properties is invoked, where we set $L_i = L$. Within this treatment, the GB energy, γ_{gb}, width,

δ_{gb}, and mobility, M_{gb}, are uniquely determined via (Abdeljawad and Foiles, 2015).

$$\gamma_{gb} = \frac{2\sqrt{2}}{3}\,\epsilon\,\sqrt{W_\phi}, \tag{4}$$

$$\delta_{gb} \simeq \frac{1.1}{\sqrt{2}}\frac{\epsilon}{\sqrt{W_\phi}}, \tag{5}$$

$$M_{gb}\gamma_{gb} = L\epsilon^2. \tag{6}$$

Systems are discretized to produce a uniform grid of $N_x \times N_y \times N_z$ voxels in 3D ($N_x \times N_y$ pixels in 2D), where the voxel size is $\Delta x = \Delta y = \Delta z = 1.0$, along the x, y and z directions, respectively. Here, ϵ and W_ϕ are chosen such that the interface width is resolved by six grid points, which provides a good compromise between accuracy and computational tractability. The PF governing equations, i.e., Eqs. 3, are solved using explicit Euler method for the time derivatives and central finite differencing with the Moore stencil for spatial gradients. Periodic boundary conditions along all spatial dimensions for all fields are used. In all PF simulations presented in this work, we set $(\epsilon, W_\phi, L) = (2.0, 0.25, 1.0)$ and unless otherwise stated the phase fields were initialized by setting $\phi_i(\mathbf{r}, t = 0) = 0.5 + \xi(\mathbf{r})$, where $\xi \in [-0.2, 0.2]$ is a random number. A typical output of these simulations is a realization of grains in a polycrystalline system, where the vector of the phase fields $\{\phi_i(\mathbf{r}, t), i = 1, \cdots, n_\phi\}$ is resolved at each voxel in the simulation domain.

2.2. Conformal meshing technique

To generate a conformal mesh from a uniform grid of PF data, the Sculpt meshing tool (Owen et al., 2011) is used. Sculpt is a companion application to the Cubit Meshing and Geometry Toolkit developed at Sandia National Laboratories. It is a parallel all-hex tool that utilizes an overlay grid procedure where smooth conforming grain interfaces are extracted from PFs. In this work, the PF values are treated as volume fractions of grains, where we note that $\phi_i = 0$ or 1 corresponds to equilibrium bulk grain regions, while $\phi_i \in (0, 1)$ define GBs, where for simplicity $\phi_i = 0.5$ is used to locate the center of the GB. The procedure is briefly outlined in panels (a) through (d) of Fig. 1. Figure 1 (a) shows an example of a Cartesian grid of volume fractions where v_i is the volume fraction of the i^{th} grain contained within each grid cell. Thus, $\sum v_i = 1.0$ is satisfied. Grain interfaces are approximated using a procedure described in (Owen et al., 2011) and grid nodes are moved to the interfaces as shown in Fig. 1 (b). A layer of hexahedra is inserted on both sides of

the grain interfaces by projecting orthogonally from the local interface tangent plane. To improve mesh quality, a smoothing step is performed to improve both smoothness of the interface planes and the quality of the hexahedra as shown in Fig. 1 (d). Figure 2 shows schematics of the pillowing procedure that improves mesh quality at interfaces.

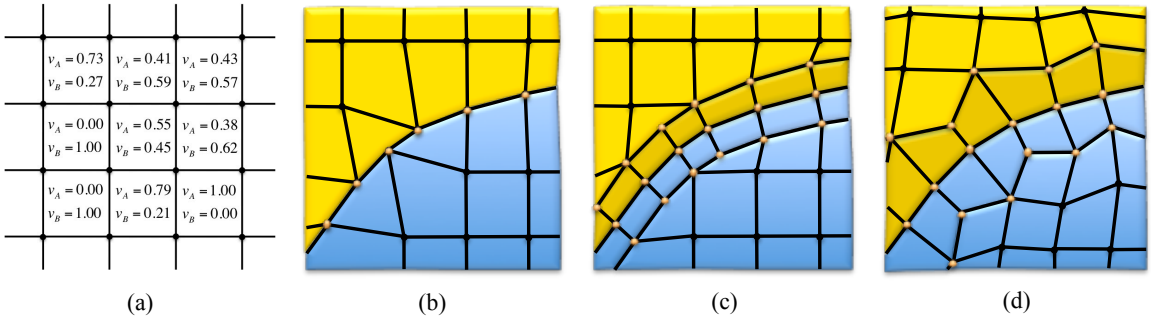

Figure 1: Schematics of the conformal meshing procedure: (a) Volume fractions representing percent of grains filling each cell in Cartesian grid, (b) grain interfaces are resolved and nodes projected to surfaces, (c) layer of hex element inserted on both sides of interface surfaces and (d) smoothing performed on curves, surfaces and volume nodes.

We note that the projection procedure illustrated in Fig. 1 may result in hexahedra where more than two nodes of a face are projected to a curve. In these cases, smoothing alone is unable to improve mesh quality to an acceptable range. To accommodate this, an additional pillowing (Mitchell and Tautges, 1995) procedure is employed. Figure 2 illustrates the procedure where a continuous layer of hexes is inserted around groupings of hexes known as *shrink sets*. Each shrink set is defined by the set of hexes immediately adjacent a common surface. With the pillow layers inserted, additional smoothing is performed to optimize element quality.

The above procedure allows for cases where multiple grains meet at common interfaces. To accommodate this, an underlying boundary representation (B-Rep) consisting of vertices, curves, surfaces and volumes is constructed which serve as the basis for smoothing operations. Nodes on curves are smoothed and projected to a Hermite approximation of the surrounding curve nodes. Surfaces are then smoothed using a Laplacian smoothing procedure. Volume nodes are then smoothed using a combined Laplacian and Optimization-based procedure described in (Owen, 2013). Several iterations of curve, surface and volume smoothing are performed until a minimum mesh quality metric is achieved. As mesh quality is a critical factor in this procedure, we note instances where the grain interfaces may intersect the domain boundary at very small angles consequently resulting in hexes that also have very small dihedral angles as shown in Fig. 3 (a). To address this issue,

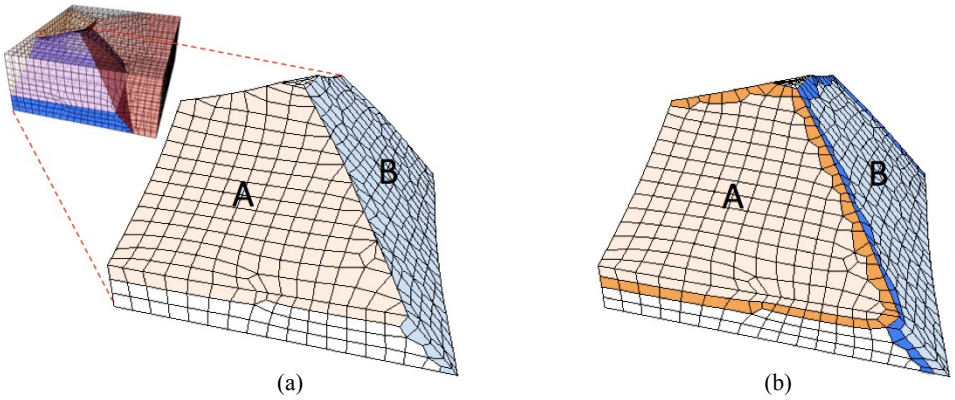

Figure 2: Schematics of the pillowing procedure: (a) Initial mesh at curve interfaces may be poor. Note triangle shaped quad faces between surfaces A and B. (b) Pillow layers of hexes are inserted srrounding all hexes sharing a common surface. Darker hexes indicate pillow layers. Note improved quad faces at curve between surfaces A and B compared to (a).

Fig. 3 (b) illustrates where additional layers of Cartesian cells can be added at the boundary of the domain. To facilitate this, volume fractions from the original boundary are copied to the new layers. This results in interfaces that intersect with the boundary at angles closer to ninety degrees, resulting in improved quality hexes.

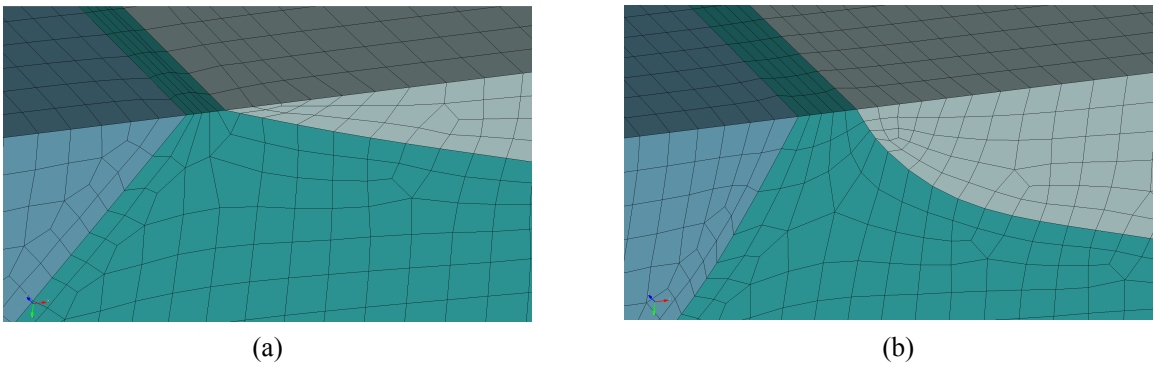

Figure 3: Mesh quality improvements: (a) Poor quality hexes may result where grain interfaces intersect domain boundaries at small angles. (b) Additional layers of cells added to the domain boundaries result in improved quality for case illustrated in (a).

2.3. Crystal plasticity finite element model

In this work, a BCC crystal plasticity finite element (CP-FE) model developed at Sandia National Laboratories (Lim et al., 2013, 2015b) is used to simulate the mechanical behavior and plastic deformation of polycrystalline α-iron. Crystal plasticity models use constitutive descriptions and

crystal orientations applied to individual grains and impose plastic slip along specified slip systems. The model used in this work is based on a well-established continuum formulation following a multiplicative decomposition of the deformation gradient (Lee, 1969; Rice, 1971; Hill and Rice, 1972; Peirce et al., 1982; Dingreville et al., 2010; Lim et al., 2014, 2015a). Assuming plastic deformation is caused by dislocation slip, the plastic part of the velocity gradient, $\mathbf{L}_\mathrm{p}$, can be written as (Peirce et al., 1982):

$$\mathbf{L}_\mathrm{p} = \sum_\alpha \dot{\gamma}^\alpha \mathbf{s}_0^\alpha \otimes \mathbf{n}_0^\alpha, \tag{7}$$

where $\mathbf{s}_0^\alpha$ and $\mathbf{n}_0^\alpha$ are the initial slip direction and the slip plane normal direction on the α-th slip system, respectively. Here, 24 $\{110\}\langle 111\rangle$ slip systems are used and for simplicity, non-Schmid effects are neglected. The slip rate on α-th slip system, $\dot{\gamma}^\alpha$, is represented as a power-law function of resolved shear stress, τ^α, and slip resistance, g^α (Hutchinson, 1976):

$$\dot{\gamma}^\alpha = \dot{\gamma}_0^\alpha \left(\frac{\tau^\alpha}{g^\alpha}\right)^{1/m}, \tag{8}$$

where $\dot{\gamma}_0^\alpha$ is the reference shear rate and m is the rate sensitivity factor. The slip resistance, g^α, is composed of thermal (τ^*) and athermal (τ_{obs}) parts as follows (Lim et al., 2015a):

$$g^\alpha = \sqrt{(\tau^*)^2 + (\tau_\mathrm{obs})^2}, \tag{9}$$

where,

$$\tau^* = \tau_{cr}\left(1 - \left(\frac{k_b T}{H_0}\ln(\dot{\epsilon}_0/\dot{\gamma})\right)^{1/q}\right)^{1/p} \text{ and } \tau_\mathrm{obs} = A\mu \mathrm{b}\sqrt{\sum_{\beta=1}^{\mathrm{NS}} \rho^\beta}. \tag{10}$$

Here, T is the temperature, $\dot{\gamma}$ is the strain rate, H_0 is the activation enthalpy, k_b is the Boltzmann's constant, τ_{cr}, $\dot{\epsilon}_0$ p, q and A are material constants, μ is the shear modulus, b is the Burger's vector, NS is the total number of slip systems, and ρ^β is the dislocation density on slip system β. Note that τ^* represents the temperature and strain rate dependent lattice resistance term based on dislocation-kink pair theory (Seeger, 1981, 2001; Argon, 2008; Butt, 2007; Lim et al., 2015a) while τ_obs is the athermal resistance to slip governed by dislocation-dislocation or dislocation-

obstacle interactions. It is assumed that the initial dislocation densities are identical for all 24 slip systems and the evolution of dislocation density for the α-th slip system is obtained by a standard phenomenological equation (Kocks, 1976). Detailed formulation of the model and material parameterizations for α-iron can be found in (Lim et al., 2015b).

3. Results and Discussion

Simulation results of 2D and 3D grain ensembles are presented. Herein, we examine the following three cases: (1) An idealized spherical grain embedded in a matrix grain, (2) a 2D polycrystalline aggregates with various grain sizes, and (3) a 3D polycrystalline aggregate. These systems were chosen because they span various degrees of geometric complexity. The CP-FE framework is used to investigate the elasto-plastic deformation of each case. Moreover, the effects of conformal and the widely-used voxelated FE discretizations on the local mechanical behavior are examined and quantified.

3.1. Case I: Spherical grain within a cubic matrix

A two-grain microstructure is constructed, where a spherical grain is embedded inside a cubic grain as shown in Fig. 4(a). This microstructure represents one of the most geometrically simple grain realizations, and is mainly used to demonstrate our modeling capability and better quantify the role of interface mesh smoothness (conformal vs. voxelated) on the local fields. The two PF equations, for the order parameters ϕ_1 and ϕ_2, were solved on a uniform mesh with $N_x = N_y = N_z = 80$ for a few steps in order to generate diffuse interfaces. Grain 1 represents the matrix grain with $(\phi_1, \phi_2) = (1, 0)$, while grain 2 is the spherical one with $(\phi_1, \phi_2) = (0, 1)$. Both ϕ_1 and ϕ_2 change rapidly but smoothly across the GB, where $\phi_1, \phi_2 \in (0, 1)$ [cf. Fig. 4(a)]. Voxelated and conformal FE discretizations are generated with a total of 512,000 (30,047 in the spherical grain) and 540,248 (44,171 in the spherical grain) eight-noded hexahedral FE elements, respectively. These discretizations are shown in Fig. 4(b) and (c) for the voxelated and conformal meshes, respectively. It can be clearly seen from Fig. 4(c) that the conformal mesh accurately represents the smooth curvature of the sphere, while the voxelated one poorly represents the interface even with a relatively fine element size. The two FE discretizations shown in Fig. 4 are used as input structures for the CP-FE model, parameterized to α-iron, to simulate uniaxial tension. Utilizing the Bunge convention

for Euler angles, the initial crystal orientation of Grain 1 was set to $(\varphi_1, \Phi, \varphi_2) = (0°, 0°, 0°)$, while for Grain 2 it was set to $(\varphi_1, \Phi, \varphi_2) = (90°, 135°, 54.7°)$. Displacements along the x-direction are applied up to 10% engineering strain at a nominal strain rate of 10^{-4} s^{-1}.

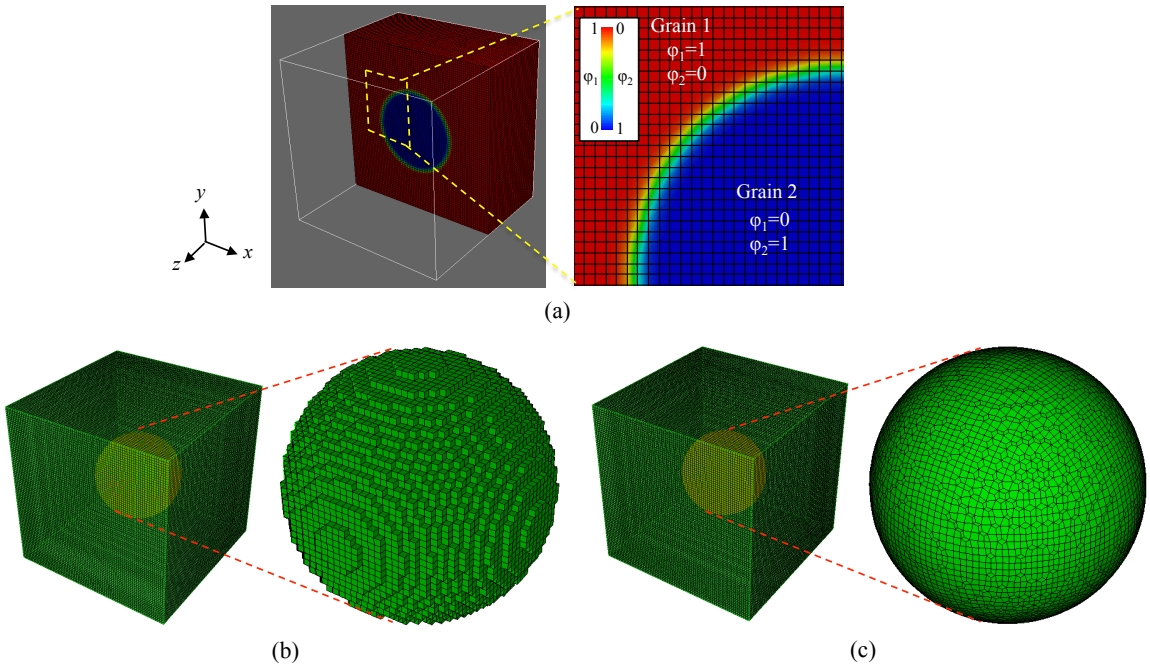

Figure 4: A two-grain system, where a spherical grain (Grain 2) is embedded in a matrix grain (Grain 1). (a) Phase field representation, where half of the system is removed for better visualization. The corresponding FE discretizations using (b) voxelated mesh and (c) conformal one, which ensures smoothness across interfaces between the two adjoining grains.

Figure 5(a) shows simulated stress-strain curves of the bicrystal using the two FE discretizations. It is shown that the type of mesh (voxelated/conformal) has negligible effect on the macroscopic response, less than 0.1% deviation in engineering stress at 10% deformation. Figure 5(b) displays contours of the von Mises stress at 10% nominal deformation using both voxelated and conformal FE discretizations. It can be seen that the overall stress distribution within Grain 1 is similar in both discretizations, but higher stress localization is observed for the voxelated mesh. Despite the geometrically simple interface between the two grains, regions close to this interface are under a higher state of stress in the voxelated system than the conformal one. To quantify this localization effect, a slice in the $x - y$ plane that is centrally located along the z-direction is extracted. Then, the von Mises stress at the elements that are spatially located at the interface between Grains 1 and 2 [cf. Figs. 6(a) and (b)] is plotted tangentially and shown in Fig. 6(c). It can be seen that

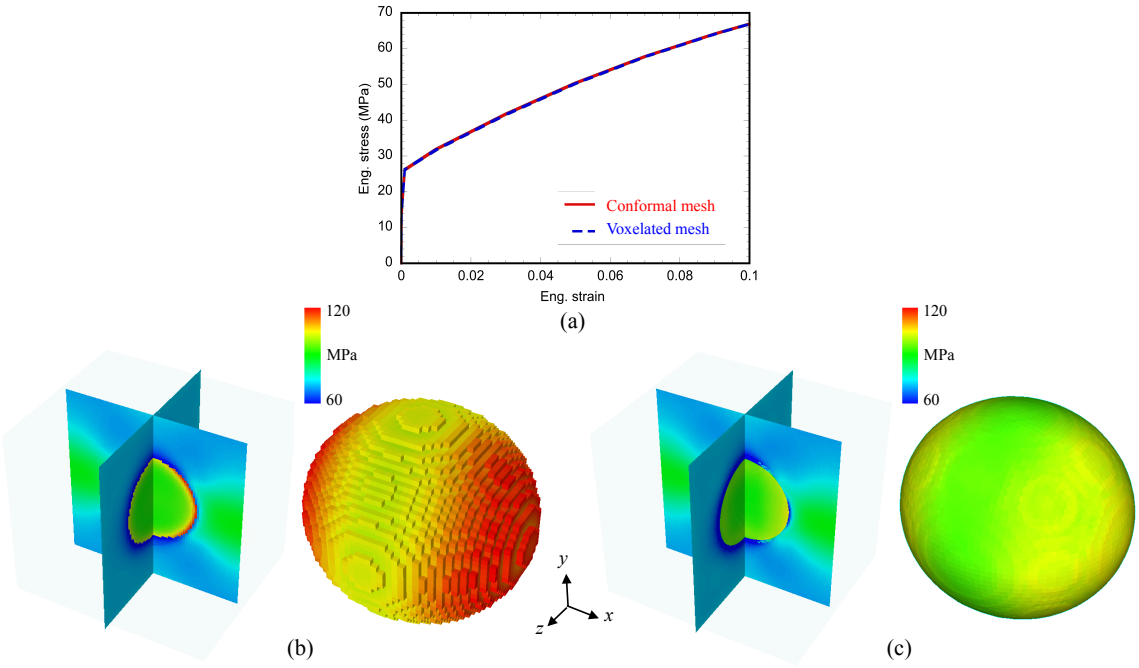

Figure 5: (a) A plot the predicted stress-strain curves of the two-grain system using conformal and voxelated FE meshes. Contours of von Mises stress at 10% nominal deformation for the system with (b) voxelated and (c) conformal FE discretizations.

the voxelated FE mesh yields stresses that are $\sim 15\%$ higher than the system with conformal FE mesh. The results shown in Figs. 5 and 6 indicate that even for some of the most geometrically simple interfaces, variations in the local state of stress exist due to the FE discretization at such interfaces. These local variations do not appear in macroscopic measures such as the global stress-strain response. Such local effects may play a significant role in continuum-based models of failure, i.e., nucleation of cracks, voids and damage. Therefore, ensuring that local stresses are convergent and not influenced by the numerical discretization is key when considering such complex processes.

3.2. Case II: Two-dimensional polycrystals

The second test case we examine in this work represents a series of 2D microstructures, where the PF equations were solved on a uniform grid with $N_x = N_y = 256$ pixels and $n_\phi = 100$. These microstructures effectively represent a simulated anneal process where the average grain size grows with time. Here, four snapshots corresponding to a non-dimensional phase field simulation time, t^*, of 80, 216, 384 and 1176 were utilized and are shown in panels (a) through (d) of Fig. 7, respectively. For the purpose of visualization, in Figs. 7(a)-(d) we plot the field $\Psi = \sum_{i=1}^{n} \phi_i^2 \left(1 - \phi_i\right)^2$ which takes

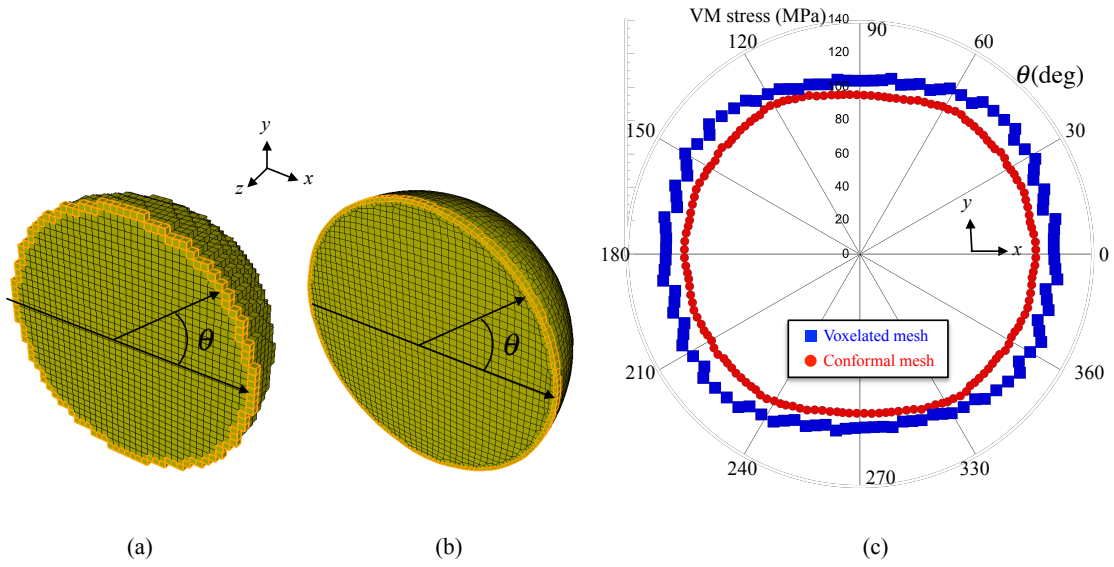

Figure 6: At 10% nominal deformation along the x direction, variation of von Mises stress tangentially, in voxelated and conformal meshes, along FE separating Grains 1 and 2, in the $x-y$ plane, at the center slice along the z direction.

a finite value within GBs (red) and changes smoothly to zero in the bulk grains (blue). In these systems, the resulting number of grains was 127, 59, 36 and 16, corresponding to Fig. 7(a) through (d), respectively.

The resulting conformal FE discretizations have $\sim 200,000$ hexahedral finite elements and are shown in Figures 7(e)-(h) for the corresponding ones in panels (a)-(d), respectively. Figure 8(a) depicts the PF representation of the microstructure shown in Fig. 7(a) along with a closeup view at one of the GB regions, while Fig. 8(b) shows the corresponding FE discretization, where it can be seen that FE elements conform to the grain topology and ensure smoothness of the interfaces between adjoining grains. It is worth noting that since the isotropy assumption for the interfaces is assumed in the phase field model, balance of interfacial tensions at triple junctions, where three grains meet, yields angles of 120°. This configuration is preserved in the conformal FE discretization as depicted in Fig. 8(b).

Next, the mechanical behavior of the microstructures shown in Fig. 7 is examined. Using the Bunge convention for Euler angles, the initial crystallographic orientations of each grain are assigned randomly and these systems are deformed up to 10% nominal strain along the x-direction at a nominal strain rate of $10^{-4}\ \mathrm{s}^{-1}$. Figure 9(a) is a plot of the predicted stress-strain curves of these systems. It is shown that flow stress is increased with decreasing grain sizes despite the fact that

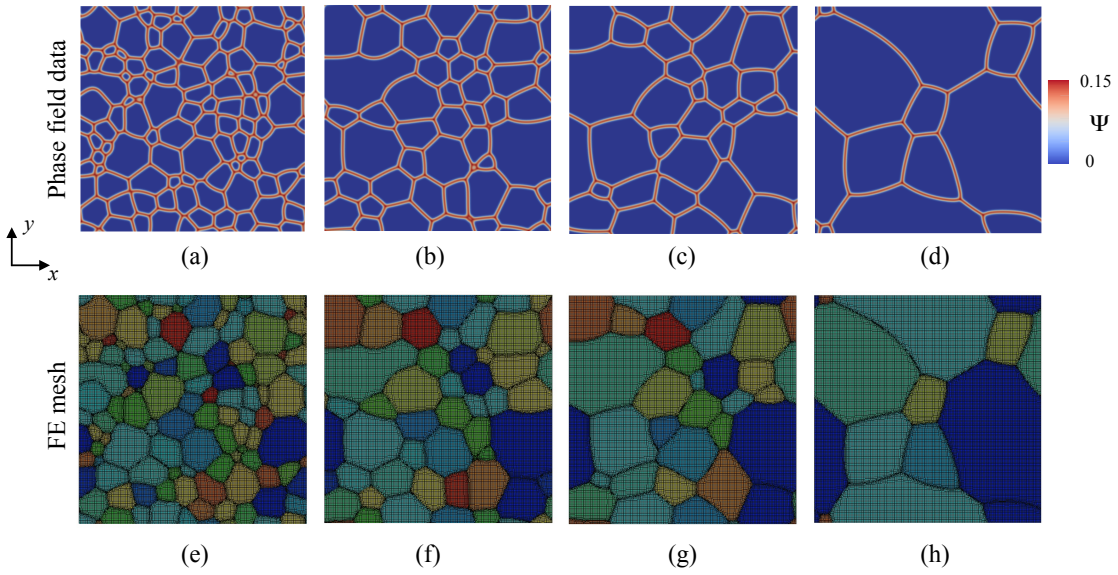

Figure 7: Snapshots of the PF microstructures [(a)-(d)] and the corresponding FE discretizations [(e)-(h)] at a non-dimensional simulation time of 80 [(a) and (e)]], 216 [(b) and (f)], 384 [(c) and (g)] and 1176 [(d) and (h)] having 127, 59, 36 and 16 grains, respectively..

the current CP-FE model does not incorporate non-local effects, i.e., the Hall-Petch effect, twhich would require considerations of dislocation-dislocation and dislocation-GB interactions. The slight variation in the macroscopic stress-strain response of these systems may be attributed to local grain orientations and neighboring effects, i.e., due to the finite number of grains used in these simulations. Figures 9(b)-(e) show contour maps of von Mises stress at 10% nominal deformation for the four microstructures depicted in Figs. 7(a)-(d), respectively. It can be seen that stress is localized near GBs and at triple junctions and this localization effect is more profound in microstructures with smaller grains. The spatial localization of the deformation [cf. Fig. 9(b)-(e)] at various microstructural features, such as GBs and triple junctions, is an indication that physically-based representations of materials microstructures and the corresponding accurate FE discretizations may be an important aspect when local effects drive complex failure processes in metals (i.e., nucleation of cracks/voids).

3.3. Case III: Three-dimensional polycrystals

We now turn our attention to 3D microstructures. First, the PF equations were solved on a uniform grid of $N_x = N_y = N_z = 96$ with $n_\phi = 20$. A realization of a representative microstructure is shown in Fig. 10(a), where the total number of grains is 52. Numerical FE discretizations of this

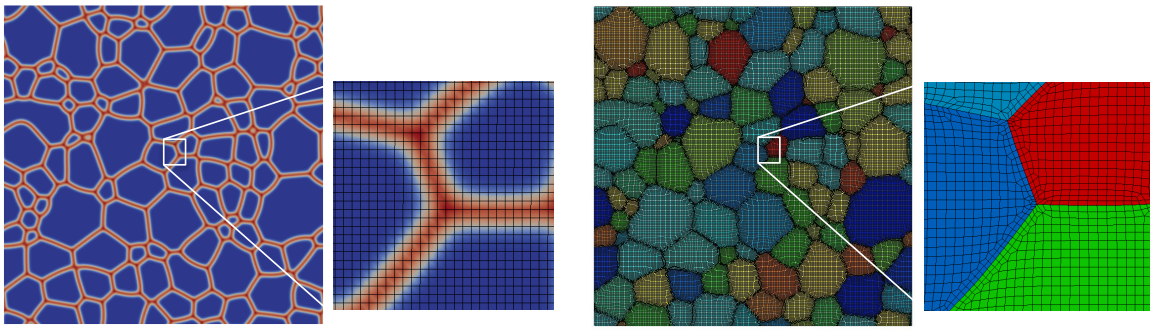

Figure 8: For the microstructure shown in Fig. 7(a): (a) phase field representation using the Ψ field where red (blue) denote (GBs) bulk grains. (b) FE discretizations of the microstructure. Curved grain boundaries and triple junction angles are accurately reproduced by the conformal FE mesh.

microstructure using both voxelated (884,736 hexahedral FE) and conformal (1,277,808 hexahedral FE) techniques are depicted in Fig. 10(b) and (c), respectively, where the mesh of only one grain is shown for better visualization. It can be seen that the smooth curved surfaces of individual grains are accurately captured by the conformal mesh. Uniaxial tension of the 3D polycrystalline system is simulated using voxelated and conformal FE meshes, where displacements along the x-direction are applied up to 10% engineering strain at a nominal strain rate of 10^{-4} s^{-1}.

Figure 11(a) is a plot of the stress-strain curves for the 3D system using both FE discretizations, conformal and voxelated. Similar to the two cases studied above, CP-FE simulations using conformal and voxelated FE discretizations show relatively small variations in the macroscopic response. Contours of the von Mises stress for these systems are shown in Figs. 11(b)-(c) for the voxelated and conformal meshes, respectively. As an illustration, in the grains labeled 11 and 15, it is clear that the conformal mesh yields a more detailed and smooth stress distribution, especially near the GBs and triple junctions. On the other hand, non-smooth and local spikes in the stress exist in the system with voxelated mesh. The local spikes in stress follow patterns that are set by the inherent voxelated mesh (notice the stress profile in grain 11).

In addition to the local mechanical response, the effects of FE mesh on texture evolution are investigated by plotting crystal orientations before and after in rolling direction (RD), transverse direction (TD) and normal direction (ND) within the unit stereographic triangle. Figure 12 shows plots of initial (black data points) and deformed texture (color contours). Here, an occurrence of crystal orientation data within a unit area of the stereographic triangle is normalized by the

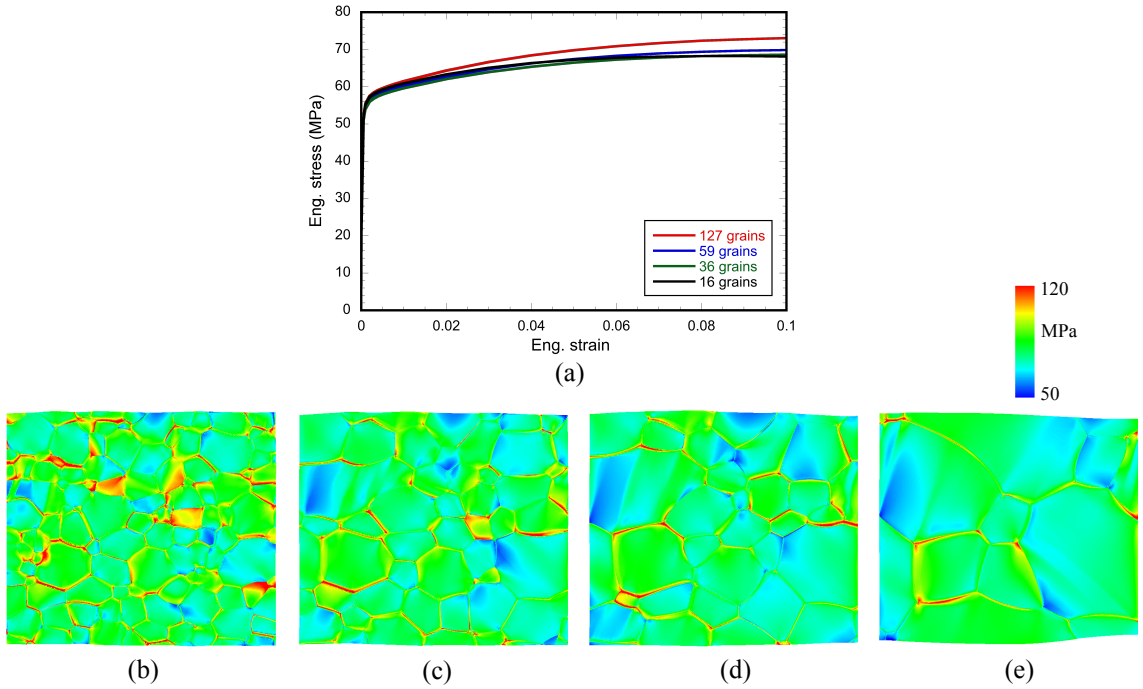

Figure 9: For the microstructures shown in Figs. 7(a)-(d). (a) Plot of the predicted stress-strain curves. (b)-(e) Contours of von Mises stress at 10% deformation for the microstructures in Figs. 7(a)-(d), respectively. Notice the localized deformation at grain boundaries and triple junctions.

random occurrence. The spread in the initial crystal orientations within a grain are observed in the deformed texture. Similar to the macroscopic stress-strain response, overall predicted texture using voxelated and conformal FE discretizations shows good agreement.

Next, we quantitatively examine the local stress fields that are predicted from the two meshing techniques. To this end, a slice in the x-y plane centrally located along the z-axis is conveniently picked [cf. Fig. 13(a)]. Then, within this slice, the von Mises stress is extracted along a line that extends along the x-axis [black line in Fig. 13(a)], where the points labeled A and B correspond to a GB and triple junction, respectively. The von Mises stress values along this line scan in the systems with voxelated and conformal meshes are shown in Fig. 13(b). It can be seen that differences in the local state of stress between voxelated and conformal FE discretizations exist at regions with an abrupt change in the materials properties. The state of stress far from these regions is similar in both systems (voxelated and conformal). At the GB, point A in Fig. 13(b), a jump in the von Mises stress exists for the system with conformal mesh due to the abrupt change in the elastic moduli. Furthermore, at the triple junction, point B, a spike in the von Mises stress is observed in

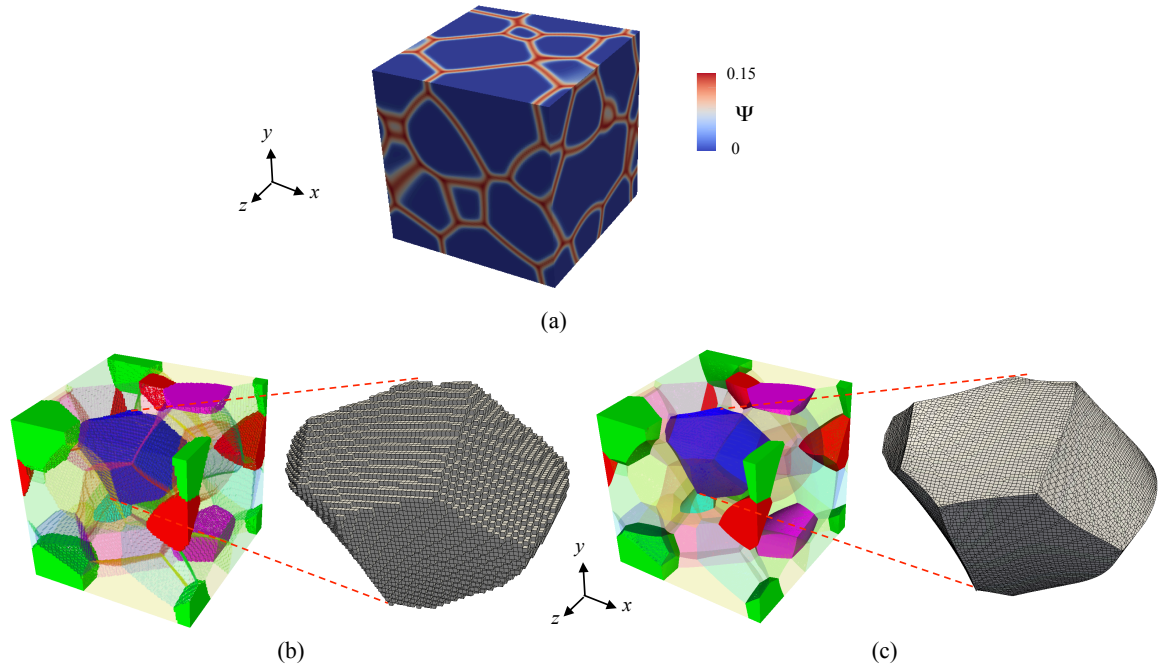

Figure 10: (a) Phase field representation of the 3D grain microstructure. The scalar field Ψ is used for visualization, where (red) blue denote (GBs) bulk grains. FE discretization of the microstructure in (a) using (b) voxelated, and (c) conformal meshing techniques.

the system with the voxelated mesh, whereas the one with the conformal mesh yields a spatially smoother stress around this point. In this case, the stress at point B in the system with voxelated FE discretization is $\sim 65\%$ higher than the one with conformal mesh. Therefore, one expects that the effects shown in Fig. 13(b) may influence the behavior when local effects are considered in models of failure.

3.4. Anticipated impact

The modeling approach presented in the study bridges a mesoscale model of grain microstructures in polycrystalline metals to one of the mechanical properties, i.e., elasto-plastic deformation, where attention has been focused on accurately representing the various features of such systems (grain topology, smooth interfaces). This unique modeling capability can be extended to incorporate realizations from mesoscale models of various materials processes, such as coarsening of multi-phase multi-component systems, solidification and dendritic growth, and additive manufacturing processes, into continuum models of the deformation behavior and failure mechanisms in these systems. Moreover, the capability can be applied to use microstructures obtained experi-

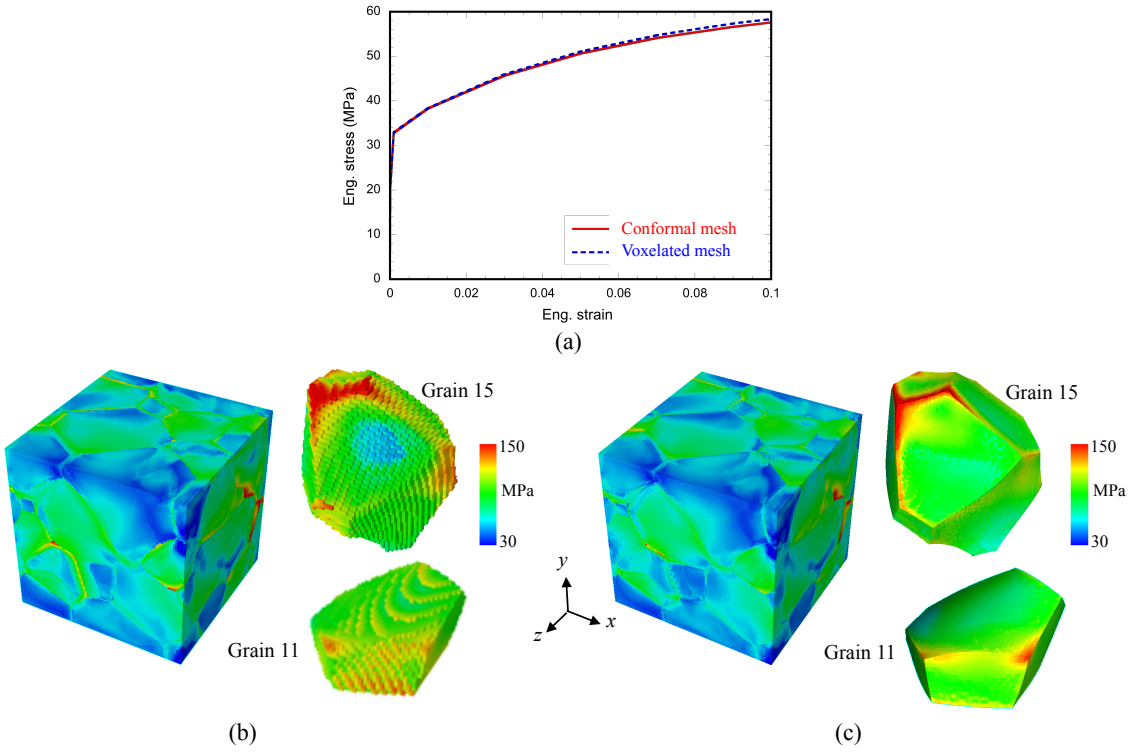

Figure 11: For the 3D polycrystalline microstructure in Fig. 10(a). (a) Plot of the stress-strain curves using both voxelated and conformal meshes. Contours of von Mises stress at 10% deformation using (b) voxelated and (c) conformal meshes. In the grains labeled 11 and 15, notice the non-smooth and localized stress due to the voxelated mesh.

mentally, e.g., electron backscatter diffraction (EBSD). As a demonstration, Fig. 14(a) shows a representative microstructure from a phase field treatment of multi-phase coarsening of binary metallic systems, where the surface energies of both metals were set the same. Figure 14(b) is a close-up view of the FE discretization of this system, where it can be seen that the mesh conforms to the phase boundary between the two metallic phases.

Another application of our modeling approach is additive manufacturing processes, with solidification dynamics being one possible process. To this end, we utilized the PF treatment of non-isothermal solidification of a pure metal by Koboyashi (Kobayashi, 1993) to generate complex dendritic structures such as the one depicted in Fig. 15(a) and (b). The conformal meshing technique is used to generate a FE discretization, shown in Fig. 15(c), which in turn can be used in CP-FE frameworks to simulate the deformation behavior of such systems. The accurate representation of various microstructural features, such as grain shapes and sizes, and interfaces, may prove an important step towards the development of failure models that are informed by the local state

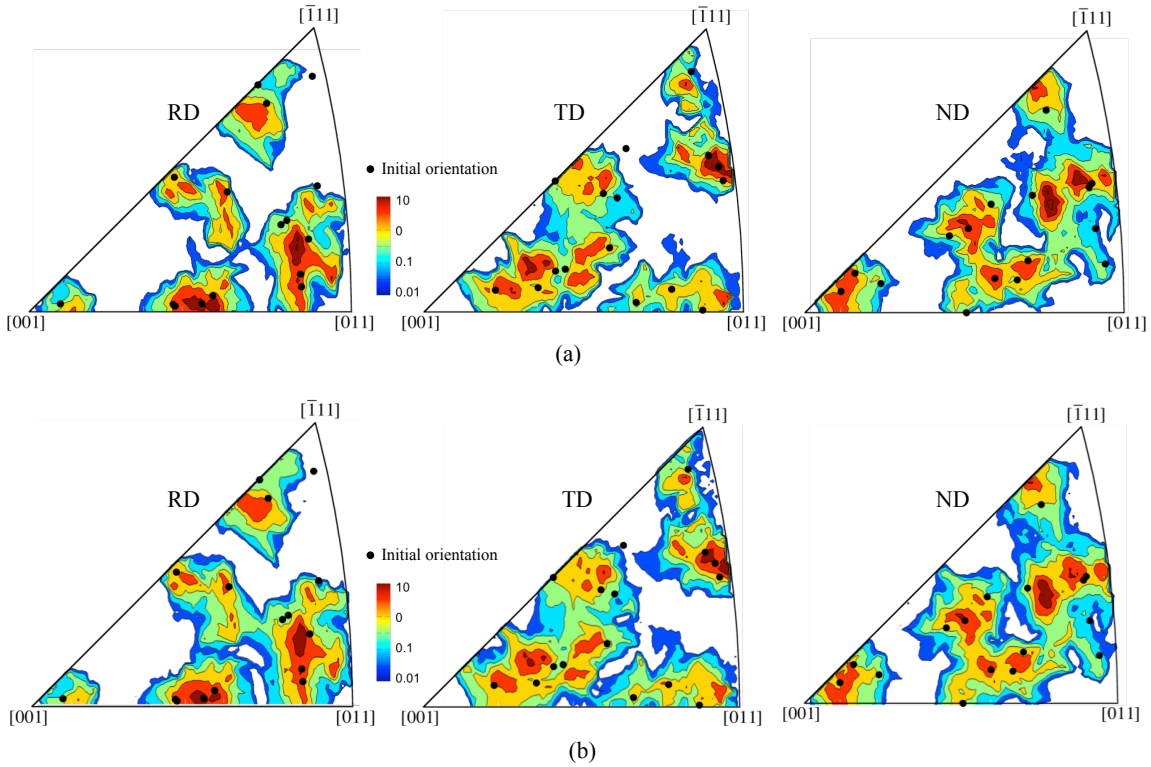

Figure 12: Crystal orientations before and after in rolling direction (RD), transverse direction (TD) and normal direction (ND) within the unit stereographic triangle. Predicted texture density plots from CP-FEM predictions using (a) voxelated and (b) conformal FE meshes. Color scale represents the multiple times random occurrence at 10% nominal deformation.

of deformation.

4. Conclusion

Concurrent trends in a wide variety of technologies are moving towards component miniaturization and increased realism in predictive simulations. This necessitates microstructure-aware engineering analysis capabilities for a variety of applications. In order to better incorporate microstructures in continuum scale treatments, a modeling framework was proposed, where realizations from a phase field model of grain microstructures were incorporated into a crystal plasticity finite element framework of the elasto-plastic deformation of polycrystalline metals. With the aid of a unique meshing technique, finite element discretizations of these materials microstructures were generated, which accurately represent grain topologies and ensure the smoothness of interfaces (GBs) between adjoining grains.

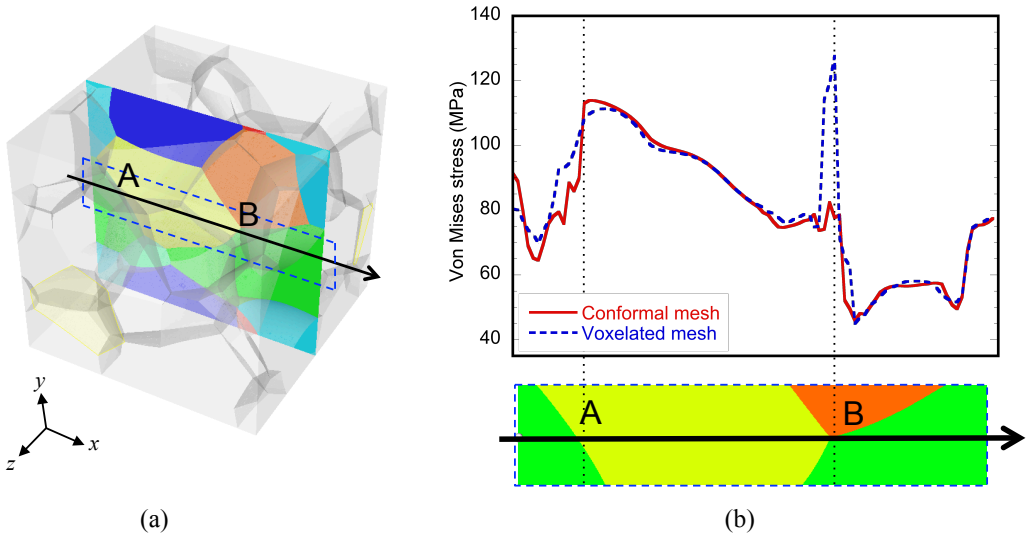

Figure 13: (a) A slice in the x-y plane centrally located along the z-axis is conveniently picked and the von Mises stress along the solid black line is extracted. (b) At 10% nominal deformation, profile of von Mises stress along the solid black line in the systems with voxelated and conformal meshes. Points labeled A and B correspond to a GB and triple junction, respectively.

Simulated annealing via the phase field model yielded a number of 2D and 3D systems with various grain shapes and sizes. FE discretizations of these microstructures using both voxelated and conformal techniques were used in the CP-FE framework to simulate the mechanical behavior of these systems. While the macroscopic behavior, through the stress-strain curves and texture plots, seemed insensitive to the degree by which interfaces between adjoining grains were numerically represented and resolved, i.e., voxelated vs. conformal, it was observed that differences in the local response exist due to such discretization effects. Systems with voxelated mesh near interfaces yielded larger stresses at GBs and triple junctions. This effect became more pronounced with the increased complexity of the microstructure. Thus, mesoscale models of failure, such as nucleations of cracks/voids, may require using interface conformal mesh in order to eliminate artificial behavior due to such numerical discretizations.

Our framework provides a step towards an integrated computational materials engineering approach, where models of materials processes are bridged to ones of properties. This enables a design loop such that models of materials properties provide key inputs to ones of processes in order to engineer materials systems with optimal performance.

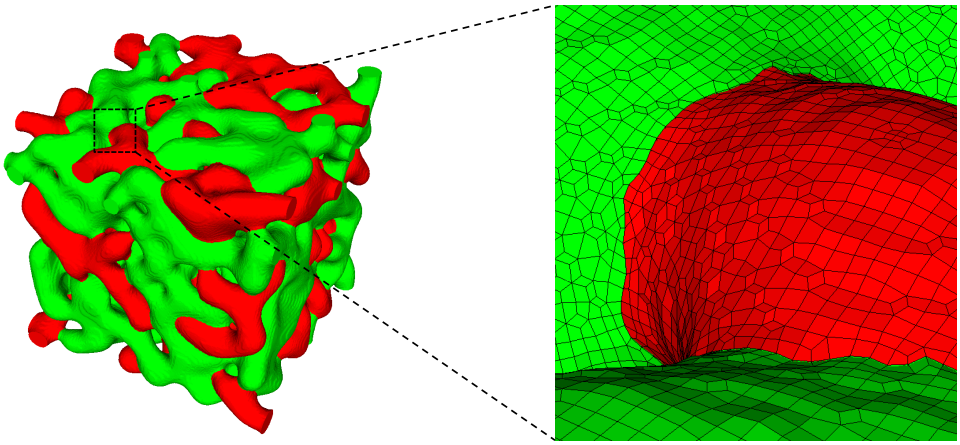

(a) (b)

Figure 14: Application of our modeling approach to multi-phase systems. (a) Phase field representation of a metallic multi-phase coarsened microstructure. (b) A close-up view demonstrating the conformal FE discretization at a phase boundary between the two metallic phases. In both panels, green (red) denote two distinct pure metallic phases.

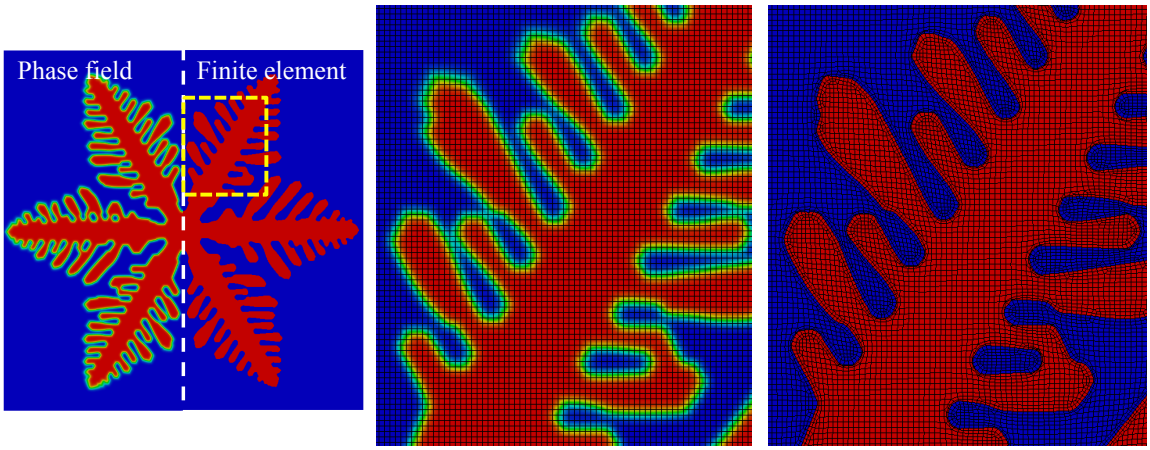

(a) (b) (c)

Figure 15: Application of our modeling approach to solidification dynamics. (a) phase field and FE representation of a dendritic microstructure with six-fold anisotropy for the interface energy. A close-up view at one of the dendrite branches [the region bounded by the dashed yellow rectangle in (a)] showing the (b) phase field profile and (c) conformal FE discretization.

Acknowledgement

Sandia National Laboratories is a multi-program laboratory managed and operated by Sandia Corporation, a wholly owned subsidiary of Lockheed Martin Corporation, for the U.S. Department of Energy's National Nuclear Security Administration under contract DE-AC04-94AL85000.

References

Abdeljawad, F., Foiles, S. M., 2015. Stabilization of nanocrystalline alloys via grain boundary segregation: A diffuse interface model. Acta Mater.In press.

Abdeljawad, F., Voelker, B., Davis, R., McMeeking, R. M., Haataja, M., 2014. Connecting microstructural coarsening processes to electrochemical performance in solid oxide fuel cells: An integrated modeling approach. J. Power Sources 250, 319–331.

Allen, S. M., Cahn, J. W., 1979. A microscopic theory for antiphase boundary motion and its application to antiphase domain coarsening. Acta Metall. 27 (6), 1085–1095.

Anand, L., Kalidindi, S. R., 1994. The process of shear-band formation in plane- strain compression of fcc metals - effects of crystallographic texture. Mechanics of Materials 17, 223–243.

Anderson, M., Srolovitz, D., Grest, G., Sahini, P., 1984. Computer-simulation of grain-growth .1. kinetics. Acta Metall. 32 (5), 783–791.

Aoyagi, Y., Shizawa, K., 2007. Multiscale crystal plasticity modeling based on geometrically necessary crystal defects and simulation on fine-graining for polycrystal. International Journal of Plasticity 23, 1022–1040.

Argon, A., 2008. Strengthening mechanisms in crystal plasticity. Oxford University Press.

Arzt, E., 1998. Overview no. 130 - size effects in materials due to microstructural and dimensional constraints: A comparative review. Acta Mater. 46 (16), 5611–5626.

Barbe, F., Decker, L., Jeulin, D., Cailletaud, G., 2001. Intergranular and intragranular behavior of polycrystalline aggregates. *p*art 1: *f.e.* model. International Journal of Plasticity 17, 513–536.

Bishop, J., Emery, J., Field, R., Weinberger, C., Littlewood, D., 2015. Direct numerical simulations in solid mechanics for understanding the macroscale effects of microscale material variability. Comp. Meth. App. Mech. Eng. 287, 262–289.

Boissonnat, J.-D., Yvinec, M., 1998. Algorithmic Geometry. Cambridge University Press.

Butt, M. Z., 2007. Kinetics of flow stress in crystals with high intrinsic lattice friction. Philos. Mag. 87, 3595–3614.

Chen, L., 2002. Phase-fid models for microstructure evolution. Ann. Rev. of Mater. Res. 32, 113–140.

Chen, L., Yang, W., 1994. Computer-simulation of the domain dynamics of a quenched system with a large number of nonconserved order parameters - the grain-growth kinetics. Phys. Rev. B 50 (21), 15752–15756.

Dawson, P. R., MacEwen, S. R., Wu, P. D., 2003. Advances in sheet metal forming analyses: dealing with mechanical anisotropy from crystallographic texture. International Materials Reviews 48, 86–122.

Delaire, F., Raphanel, J. L., Rey, C., 2000. Plastic heterogeneities of a copper multicrystal deformed in uniaxial tension: Experimental study and finite element simulations. Acta Mater. 48, 1075–1087.

Dieter, G. E., 1986. Mechanical Metallurgy, 3rd Edition. McGraw Hill.

Dingreville, R., Battaile, C. C., Brewer, L. N., Holm, E. A., Boyce, B. L., 2010. The effect of microstructural representation on simulations of microplastic ratcheting. Int. J. Plasticity 21, 617–633.

Fromm, B., Chang, K., McDowell, D., Chen, L., Garmestani, H., 2012. Linking phase-field and finite-element modeling for process structure property relations of a ni-base superalloy. Acta Mater. 60 (17), 5984–5999.

Glimm, J., Grove, J., Li, X., Shyue, K., Zeng, Y., Zhang, Q., 1998. Three-dimensional front tracking. SIAM J. Sci. Comp. 19 (3), 703–727.

Haasen, P., 1972. Mechanical, magnetic and superconductor hardening by precipitates. Mater. Sci. Eng. 9 (4), 191–&.

Herring, C., 1951. Some theorems on the free energies of crystal surfaces. Phys. Rev. 82 (1), 87–93.

Hill, R., Rice, J. R., 1972. Constitutive analysis of elastic plastic crystals at arbitrary strain. J. Mech. Phys. Solids 20, 401–413.

Hirth, J., Lothe, J., 1982. Theory of Dislocations. Krieger.

Holm, E. A., Battaile, C. C., 2001. The computer simulation of microstructural evolution. JOM 53 (9), 20–23.

Hutchinson, J. W., 1976. Bounds and self-consistent estimates for creep of polycrystalline materials. Proc. R. Soc. Lond. A 348, 101–127.

Hyman, J., 1984. Numerical-methods for tracking interfaces. Physica D 12 (1-3), 396–407.

Kalidindi, S. R., Bronkhorst, C. A., Anand, L., 1992. Crystallographic texture evolution in bulk deformation processing of fcc metals. J. Mech. Phys. Solids 40, 537.

Kawasaki, K., Nagai, T., Nakashima, K., 1989. Vertex models for two-dimensional grain-growth. Phil Mag. B 60 (3), 399–421.

Kobayashi, R., 1993. Modeling and numerical simulations of dendritic crystal growth. Physica D 63, 410–423.

Kocks, U. F., 1976. Laws for work-hardening and low-temperature creep. J. Eng. Mater. Tech., ASME 98, 76–85.

Krill, C., Chen, L., 2002. Computer simulation of 3-d grain growth using a phase-field model. Acta Mater. 50 (12), 3057–3073.

Lazar, E., MacPherson, R., Srolovitz, D., 2010. A more accurate two-dimensional grain growth algorithm. Acta Mater. 58 (2), 364–372.

Lazar, E., Mason, J., MacPherson, R., Srolovitz, D., 2011. A more accurate three-dimensional grain growth algorithm. Acta Mater. 59 (17), 6837–6847.

Lee, E. H., 1969. Elastic-plastic deformation at finite strains. Appl. Mech. 36, 1–6.

Lim, H., Battaile, C. C., Carroll, J. D., Boyce, B. L., Weinberger, C. R., 2015a. A physically based temperature and strain rate dependent crystal plasticity model for bcc metals. J. Mech. Phys. Sol. 74, 80–96.

Lim, H., Carroll, J. D., Battaile, C. C., Buchheit, T. E., Boyce, B. L., Weinberger, C. R., 2014. Grain-scale experimental validation of crystal plasticity finite element simulations of tantalum oligocrystals. Int. J. Plasticity 60, 1–18.

Lim, H., Hale, L. M., Zimmerman, Z. A., Battaile, C. C., Weinberger, C. R., 2015b. A multi-scale model of dislocation plasticity in α-Fe: Iincorporating temperature, strain rate and non-schmid effects. Int. J. Plasticity In press.

Lim, H., Weinberger, C. R., Battaile, C. C., Buchheit, T. E., 2013. Application of generalized non-Schmid yield law to low temperature plasticity in bcc transition metals. Model. Simul. Mater. Sci. Eng. 21, 045015.

Liu, Y., Baudin, T., Penelle, R., 1996. Simulation of normal grain growth by cellular automata. Scripta Mater. 34 (11), 1679–1683.

MacPherson, R. D., Srolovitz, D., 2007. The von neumann relation generalized to coarsening of three-dimensional microstructures. Nature 446 (7139), 1053–1055.

Meier, F., Schwarz, C., Werner, E., 2014. Crystal-plasticity based thermo-mechanical modeling of al-components in integrated circuits. Computational Materials Science 94, 122–131.

Mitchell, S. A., Tautges, T. J., 1995. Pillowing doublets: refining a mesh to ensure that faces share at most one edge. In Proc. 4th International Meshing Roundtable, 231–240.

Mullins, W. W., 1956. Two-Dimensional Motion of Idealized Grain Boundaries. J. App. Phys. 27 (8), 900–904.

Nemat-Nasser, S., Hori, M., 1993. Micromechanics: Overall Properties of Heterogeneous Materials. North-Holland.

Okabe, A., Boots, B., Sugihara, K., Chiu, S. N., 2000. Spatial Tessellations: Concepts and Applications of Voronoi Diagrams. John Wiley & Sons.

Osher, S., Sethian, J., 1988. Fronts propagating with curvature-dependent speed - algorithms based on hamilton-jacobi formulations. J. Comp. Phys. 79 (1), 12–49.

Owen, S. J., 2013. Parallel smoothing for grid-based methods. Proceedings 21st International Meshing Roundtable, Research Notes.

Owen, S. J., Staten, M. L., Sorensen, M. C., 2011. Parallel hex meshing from volume fractions. Proceedings 20th International Meshing Roundtable, 161–178.

Peirce, D., Asaro, R. J., Needleman, A., 1982. An analysis of nonuniform and localized deformation in ductile single crystals. Acta Metall. 30, 1087–1119.

Phillips, R., 2001. Crystal, Defects and microstructures. Cambridge University Press.

Pyle, D., Lu, J., Littlewood, D. J., Maniatty, A. M., 2012. Effects of $3d$ grain structure representation in polycrystal simulations. Computational Mechanics 52, 135–150.

Raabe, D., M. Sachtleber, Z. Z., Roters, F., Zaefferer, S., 2001. Micromechanical and macromechanical effects in grain scale polycrystal plasticity experimentation and simulation. Acta Mater. 49, 3433–3441.

Rice, J. R., 1971. Inelastic constitutive relations for solids, an internal-variable theory and its application to metal plasticity. J. Mech. Phys. Solids 19, 443–455.

Seeger, A., 1981. The temperature and strain-rate dependence of the flow stress of body-centered cubic metals: A theory based on kink–kink interactions. Z. Metallikd 72, 369–380.

Seeger, A., 2001. Why anomalous slip in body-centred cubic metals? Mater. Sci. Eng. A 319-321, 254–260.

Srolovitz, D., Anderson, M., Grest, G., Sahini, P., 1984a. Computer-simulation of grain-growth .3. influence of a particle dispersion. Acta Metall. 32 (9), 1429–1438.

Srolovitz, D., Anderson, M., Sahini, P., Grest, G., 1984b. Computer-simulation of grain-growth .2. grain-size distribution, topology, and local dynamics. Acta Metall. 32 (5), 793–802.

Steinhauser, M., 2008. Computational Multiscale Modeling of Fluids and Solids. Springer.

Steinhauser, M. O., Hiermaier, S., 2009. A Review of Computational Methods in Materials Science: Examples from Shock-Wave and Polymer Physics. Int. J. Molec. Sci. 10 (12), 5135–5216.

Teferra, K., Graham-Brady, L., 2015. Tessellation growth models for polycrystalline microstructures. Comp. Mater. Sci. 102, 57–67.

Torquato, S., 2002. Random Hetergeneous Materials. Springer.

von Neumann, J., 1952. written discussion. In: Metals Interfaces. American Society for Metals, Cleveland, OH.

Wolfram, S., 1984. Cellular automata as models of complexity. Nature 311 (5985), 419–424.

Zhang, M., Zhang, J., McDowell, D. L., 2007. Microstructure-based crystal plasticity modeling of cyclic deformation of $ti6al4v$. International Journal of Plasticity 23, 1328–1348.

Zhao, Z., Ramesh, M., Raabe, D., Cuitiño, A., Radovitzky, R., 2008. Experimental investigation of plastic grain interaction. Int. J. Plasticity 24, 2278–2297.